

The Journal of Physiology

Different kinetic properties of two T-type Ca²⁺ currents of rat reticular thalamic neurones and their modulation by enflurane

Pavle M Joksovic, Douglas A Bayliss and Slobodan M Todorovic

J. Physiol. 2005;566;125-142; originally published online Apr 21, 2005;

DOI: 10.1113/jphysiol.2005.086579

This information is current as of September 12, 2008

This is the final published version of this article; it is available at:
<http://jp.physoc.org/cgi/content/full/566/1/125>

This version of the article may not be posted on a public website for 12 months after publication unless article is open access.

The Journal of Physiology Online is the official journal of The Physiological Society. It has been published continuously since 1878. To subscribe to *The Journal of Physiology Online* go to: <http://jp.physoc.org/subscriptions/>. *The Journal of Physiology Online* articles are free 12 months after publication. No part of this article may be reproduced without the permission of Blackwell Publishing: JournalsRights@oxon.blackwellpublishing.com

Different kinetic properties of two T-type Ca^{2+} currents of rat reticular thalamic neurones and their modulation by enflurane

Pavle M. Joksovic¹, Douglas A. Bayliss^{1,2} and Slobodan M. Todorovic¹

¹Departments of Anaesthesiology and ²Pharmacology, University of Virginia Health System, Charlottesville, VA 22908, USA

Currents arising from T-type Ca^{2+} channels in nucleus reticularis thalami (nRT) play a critical role in generation of low-amplitude oscillatory bursting involving mutually interconnected cortical and thalamic neurones, and are implicated in the state of arousal and sleep, as well as seizures. Here we show in brain slices from young rats that two kinetically different T-type Ca^{2+} currents exist in nRT neurones, with a slowly inactivating current expressed only on proximal dendrites, and fast inactivating current predominantly expressed on soma. Nickel was about twofold more potent in blocking fast (IC_{50} 64 μM) than slow current (IC_{50} 107 μM). The halogenated volatile anaesthetic enflurane blocked both currents, but only the slowly inactivating current was affected in voltage-dependent fashion. Slow dendritic current was essential for generation of low-threshold Ca^{2+} spikes (LTS), and both enflurane and nickel also suppressed LTS and neuronal burst firing at concentrations that blocked isolated T currents. Differential kinetic properties of T currents expressed in cell soma and proximal dendrites of nRT neurones indicate that various subcellular compartments may exhibit different membrane properties in response to small membrane depolarizations. Furthermore, since blockade of two different T currents in nRT neurones by enflurane and other volatile anaesthetics occurs within concentrations that are relevant during clinical anaesthesia, our findings suggest that these actions could contribute to some important clinical effects of anaesthetics.

(Resubmitted 11 March 2005; accepted after revision 14 April 2005; first published online 21 April 2005)

Corresponding author S. M. Todorovic: Department of Anesthesiology, University of Virginia Health System, Mail Box 800710, Charlottesville, VA 22908-0710, USA. Email: st9d@virginia.edu

Propagation and integration of signals in the soma and dendrites of CNS neurones are regulated, in part, by the distribution and biophysical properties of voltage-gated Ca^{2+} channels. Of these channels, special attention has been focused on studies of low-voltage-activated (LVA) or transient (T) type Ca^{2+} channels, which are proposed to boost weak synaptic signals and play an important role in synaptic integration (Magee & Johnston, 1995; Magee *et al.* 1995; Markram & Sakman, 1994). The T-type Ca^{2+} current of nucleus reticularis thalami (nRT) is a key component in generating thalamocortical oscillations involving nRT, thalamic relay and cortical neurones (Steriade *et al.* 1985; Huguenard & Prince, 1992; Destexhe *et al.* 1996; McCormick & Bal, 1997). Previous recordings from isolated nRT neurones and modelling studies (Huguenard & Prince, 1992; Destexhe *et al.* 1996) suggest that dendritic and somatic currents of nRT neurones might be different. Furthermore, molecular studies of T channels indicate that at least three different isoforms exist in CNS neurones (Perez-Reyes, 2003), raising the possibility that different

subtypes of T channel may coexist even on the same neurone. Due to different cable properties of cell soma and dendrites, proximity to synapse and different intrinsic kinetic features of T currents, these distinct currents may play different roles in the control of cellular excitability. It is thus possible that any modification of these channels by pharmacological agents, including volatile anaesthetics, in a specific part of the soma and dendritic tree might locally alter neuronal signalling processes and integrative functions.

T-type Ca^{2+} channels activate with small depolarizations of neuronal membrane, and play a crucial role in control of cellular excitability and rhythmic oscillations in thalamocortical neurones (Llinas, 1988; Huguenard, 1996; Perez-Reyes, 2003). The thalamus represents a major 'gateway' of corticothalamocortical functional connections that are essential for awareness and which are dampened during the anaesthetized state (Angel, 1991). Therefore, we hypothesized that volatile anaesthetics may suppress signalling in this crucial part of

the sensory system by targeting different classes of T-type voltage-gated Ca^{2+} channels expressed on the soma and dendrites.

We found that T-type Ca^{2+} channels have differential subcellular localization, with the slowly inactivating T-type Ca^{2+} channel expressed predominantly on dendrites, and fast inactivating T channels on the soma of the nRT neurones. The inorganic T-type Ca^{2+} -channel blocker nickel was more effective in blocking somatic fast inactivating current. In contrast, the fluorinated volatile anaesthetic enflurane more effectively blocked slowly inactivating T currents underlying low-threshold Ca^{2+} spikes and bursts of action potentials in dendrites, suggesting that diminished dendritic excitability may be a contributing cellular mechanism of general anaesthesia.

Methods

In vitro tissue slice preparation

Most of experiments were performed in 200–250 μm thick transverse rat brain slices taken through the middle anterior portion of the nRT (Paxinos & Watson, 1944). Gravid Sprague-Dawley rats were housed in a local animal facility in accordance with protocols approved by the University of Virginia Animal Use and Care Committee, and investigators adhered to the guidelines published in the NIH Guide for the Care and Use of Laboratory Animals. Young rats, aged 7–14 days, were briefly anaesthetized with halothane and decapitated, and the brains rapidly removed and placed in chilled (4°C) cutting solution consisting of (mM): 2 CaCl_2 , 260 sucrose, 26 NaHCO_3 , 10 glucose, 3 KCl, 1.25 NaH_2PO_4 , 2 MgCl_2 , equilibrated with a mixture of 95% O_2 and 5% CO_2 . A block of the tissue containing the thalamus was glued to the chuck of a vibrotome (TPI, St Louis, MO, USA), and 200–250 μm slices were obtained in a transverse plane. For recordings from dendrites we cut slices in the horizontal plane, since this orientation allowed easier visualization of proximal dendrites. The slices were incubated in 36°C oxygenated saline for 1 h prior to placing in a recording chamber that had been superfused at a rate of 1.5 ml min^{-1} . The incubating saline consisted of (mM): 124 NaCl, 4 KCl, 26 NaHCO_3 , 1.25 NaH_2PO_4 , 2 MgCl_2 , 10 glucose, 2 CaCl_2 , equilibrated with a mixture of 95% O_2 and 5% CO_2 . Slices were maintained at room temperature in the recording chamber and remained viable for at least 1 h under these conditions. Since the half-life of halothane in nerve tissue following induction of anaesthesia is only about 10 min (Stevens & Kingston, 1992), it is unlikely that anaesthetic used to kill animals could interfere with the results of our experiments that were performed at least 2 h later.

Recording procedures

The standard extracellular saline for recording of Ca^{2+} currents consisted of (mM): 2 CaCl_2 , 130 NaCl, 2.5

MgCl_2 , 10 glucose, 26 NaHCO_3 , 1.25 NaH_2PO_4 , and 1 μM TTX to block voltage-gated Na^+ currents. For recording of T-type Ca^{2+} currents, internal solution (solution 1) was used that contained (mM): 135–140 tetramethylammonium hydroxide (TMA-OH), 10 EGTA, 40 Hepes and 2 MgCl_2 , titrated to pH 7.15–7.25 with hydrogen fluoride (HF) (Todorovic & Lingle, 1998). For some experiments (Fig. 6A–D), this internal solution (solution 2) was altered by adding (mM) 3 MgATP , 0.3 Tris-GTP, 45 caesium methane-sulphonate (with decreased TMA-OH to 90), titrated with HF to pH 7.15–7.25. For recording of high-voltage-activated (HVA) Ca^{2+} currents, internal solution (solution 3) contained (mM): 110 caesium methane-sulphonate, 14 phosphocreatine, 10 Hepes, 9 EGTA, 5 MgATP and 0.3 Tris-GTP, pH adjusted to 7.15–7.20 with CsOH. Recording electrodes for current-clamp studies contained (mM): 130 KCl, 5 MgCl_2 , 1 EGTA, 40 sodium Hepes, 2 MgATP , 0.1 Na_3GTP (pH 7.2). For the data presented in this study, values of membrane potential were corrected for the measured liquid junction potential of -10 mV (solution 1), -2 mV (solution 2) and -3 mV (solution 3) in voltage-clamp experiments, and -5 mV in current-clamp experiments.

For cell-attached recordings of Ca^{2+} currents, electrodes contained: 140 mM tetraethylammonium chloride (TEA), 10 mM BaCl_2 , 2 mM MgCl_2 , 1 mM CsCl, 3 mM 4-aminopyridine, 1 μM TTX and 10 mM Hepes (pH 7.2 adjusted with Tris-base solution) (Williams & Stuart, 2000).

Whole-cell, nucleated patch and cell-attached recordings were obtained from nRT neurones visualized with an IR DIC camera (Hammamatsu, C2400) on the Zeiss 2 FS Axioscope (Carl Zeiss, Jena) with a $\times 40$ lens.

Electrophysiological recordings

We recorded Ca^{2+} currents in coronal thalamic slices from young rats from a total of 318 visually identified nRT neurones ($R_s < 20 \text{ M}\Omega$). Recordings were made with standard whole-cell and cell-attached voltage-clamp techniques (Hamill *et al.* 1981), or the nucleated patch technique (Sather *et al.* 1992). Electrodes were fabricated from thin-walled microcapillary tubes, with final resistances of 3–6 $\text{M}\Omega$ for somatic whole-cell, cell-attached and nucleated patch recordings, and 7–11 $\text{M}\Omega$ for cell-attached recordings from dendrites. Membrane currents were recorded with an Axoclamp 200B amplifier (Axon Instruments, Union City, CA, USA). Voltage commands and digitization of membrane currents were done with Clampex 8.2 of the pClamp software package (Axon Instruments) running on an IBM-compatible computer. Neurones were typically held at -100 mV and depolarized to -50 mV every 15–20 s to evoke inward T currents. Data were analysed using

Clampfit (Axon Instruments) and Origin 7.0. For whole-cell recordings, currents were filtered at 5–10 kHz, and for cell-attached and nucleated patch recordings, currents were filtered at 2–5 kHz. Series resistance was typically compensated 50–80% during experiments. In most experiments, a P/5 protocol was used for on-line leakage subtractions.

Since voltage control is compromised in whole-cell recordings from slices due to the presence of extensive cell processes, we included in our results only cells where voltage-dependent current activation was smooth; no excessive delay in the onset of current was observed, and the onset and offset kinetics depended on voltage but not on the amplitude of current. Only cells in which adequate clamp conditions were obtained using these criteria were included in the kinetic study.

We investigated T currents in different subcellular compartments of nRT cells in slices by using the nucleated patch technique (Sather *et al.* 1992). This recording configuration uncouples somatic and dendritic currents in an intact slice preparation, and allows investigation of somatic currents in isolation. With this technique, a piece of the somatic membrane usually containing the cell nucleus is slowly (5–15 min) withdrawn with a continuous negative pressure after whole-cell is established, as depicted in Fig. 1A. Shift from whole-cell to nucleated patch configuration was detected as a large increase in resistance (up to $>1\text{ G}\Omega$), with a decrease in whole-cell capacitance, both of which were easily compensated.

Dendritic arborization of nRT neurones tends to spread in planes parallel to the long axis of the nucleus, as previously described by Ramon y Cajal (1909). Thus, for the cell-attached recordings from proximal dendrites, we prepared horizontal slices of thalamus and selected nRT cells with clearly visible proximal apical dendrites (usually two, Fig. 3A). We used the method described recently for cell-attached recordings from intact thalamic relay neurones in slices (Williams & Stuart, 2000). To include data from cell-attached recordings in our analysis, recordings had to be stable for at least 5 min; electrode capacitance had to be sufficiently well compensated and seal resistance sufficiently high (range, 3–25 $\text{G}\Omega$) to allow unambiguous identification of ensemble channel currents. T-type channel activity was recognized by characteristic near-complete inactivation of current at negative voltages. This inactivation is described by a single-exponential term, while stronger depolarizations evoked more sustained currents resembling HVA ensemble channel activity, and inactivation time constant (τ) was better described with a double or triple exponential. We did not attempt to characterize this channel activity and thus, limited our measurements only to inactivating currents where inactivation was well described by a single exponential. Steps used to activate T channels in the patches were similar to those used in whole-cell experiments and

nucleated patch experiments, and ensemble T currents typically peaked at 60–70 mV from $V_h = V_{\text{rest}} - 20\text{ mV}$ (V_h , holding potential, V_{rest} , resting potential), without significant contaminating HVA channel activity. T-type Ca^{2+} currents were presented conventionally as inward currents.

Analysis of current

Current waveforms or extracted data were fitted with the ClampFit program (Axon Instruments) or Origin 7.0 (OriginLab Corporation, Northampton, MA, USA).

The voltage dependence of steady-state activation was described with a single Boltzmann distribution:

$$G(V) = G_{\text{max}} / \{1 + \exp[-(V - V_{50})/k]\}$$

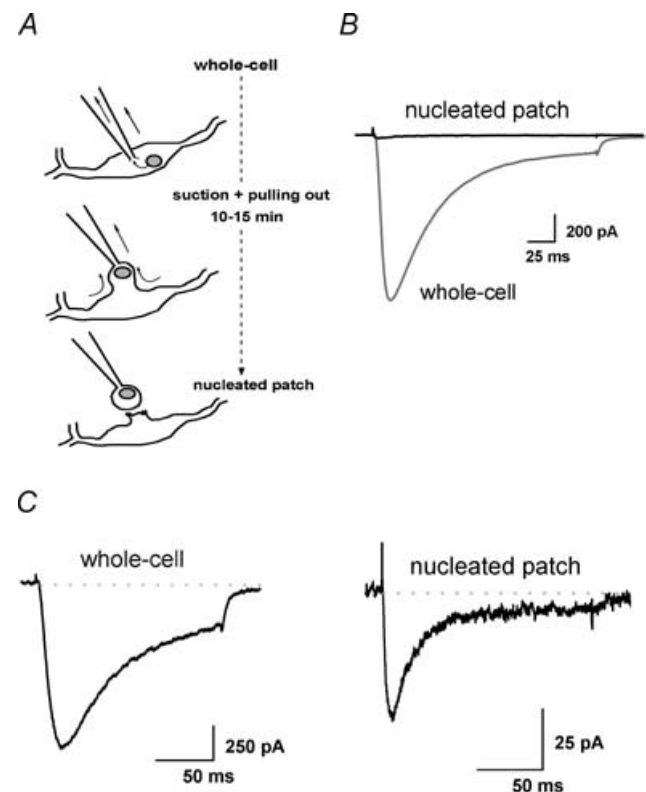


Figure 1. Distinct patterns of inactivation of T currents in nucleus reticularis thalami (nRT) neurones in whole-cell and nucleated patch recordings

A, scheme showing the tip of the electrode recording in whole-cell and nucleated patch mode (the blob represents a small piece of cell membrane surrounding the nucleus). B, the differences in T current amplitude and kinetics from whole-cell and nucleated patch recording mode evoked from holding potential (V_h) -100 mV to test potential (V_t) -50 mV in the same cell. C, scaled average traces of T currents evoked from $V_h -100\text{ mV}$ to $V_t -50\text{ mV}$ in the same cells ($n = 6$) in whole-cell and nucleated patch recordings indicate that somatic currents have faster activation and inactivation kinetics. The inactivation time constant (τ) obtained from fitting a single exponential was $54 \pm 8\text{ ms}$ in whole-cell and $18 \pm 2\text{ ms}$ in nucleated patch recordings ($P < 0.001$). The dotted line indicates zero current level.

where G_{\max} is the maximal conductance, V_{50} is the half-maximal voltage, and k (millivolts) represents the voltage dependence of the distribution.

The voltage-dependence of steady-state inactivation was described with a single Boltzmann distribution:

$$I(V) = I_{\max} / \{1 + \exp[(V - V_{50})/k]\}$$

where I_{\max} is the maximal current, V_{50} is the half-maximal voltage, and k (millivolts) represents the voltage dependence of the distribution.

Analysis of current blockade

The percentage reduction in peak T-current at a given blocker concentration was used to generate concentration–response curves. For each concentration–response curve, all points are averages of multiple determinations obtained from at least six different cells. Mean values in concentration–response curves were fitted to the following function:

$$PB([Drug]) = PB_{\max} / \{1 + (IC_{50}/[Drug])^n\}$$

where PB_{\max} is the maximal percentage block of peak T-current, the IC_{50} is the concentration that produces 50% of maximal inhibition, and n is the apparent Hill coefficient for blockade. Fitted values were typically reported with 95% linear confidence limits. Fitting was done with Origin 7.0 (OriginLab Corporation). Numerical values are given in the text as means \pm s.e.m., unless stated otherwise. Statistical analysis was performed with either Student's t test or ANOVA, with statistical significance determined with $P < 0.05$.

Drugs and chemicals

SNX-482 was obtained from Peptides International, (Louisville, KY, USA). TTX was obtained from Alomone Laboratory, Jerusalem, Israel. Sevoflurane and isoflurane were obtained from Abbott (Abbott Park, IL, USA), and enflurane was obtained from Anaquest Caribe, Inc. (Guayama, PR, USA). ω -Conotoxin GVIA, ω -conotoxin MVIIC and all other salts and chemicals were obtained from Sigma Chemical Co.

Solutions

A glass syringe served as a reservoir for a gravity-driven perfusion system that consists of multiple, independently controlled glass capillary tubes. Switching between solutions was accomplished by manually controlled valves. All experiments were done at room temperature (20–24°C). Test solutions were maintained in all-glass syringes closed with glass syringe plungers that were allowed to fall by gravity (to avoid saline evaporation

and loss of volatile agents, while maintaining rapid solution flow). All drugs were prepared as stock solutions and freshly diluted to appropriate concentrations at the time of the experiment. Aliquots of anaesthetic solutions were prepared from saturated saline solutions incubated with appropriate anaesthetic overnight (Todorovic & Lingle, 1998; Todorovic *et al.* 2000). To quantify the anaesthetic concentrations in the recording chamber, triplicate samples were analysed in a gas chromatograph (Aerograph 940; Varian Analytical Instruments, Walnut Creek, CA, USA) calibrated with appropriate volatile anaesthetic standards (Todorovic & Lingle, 1998). By measuring actual concentrations, we found a loss of less than 10% if the solution was used within 30 min from preparation. Thus, all anaesthetic solutions were used in our experiments within 30 min from preparation.

During an experiment, solution was removed from the end of the chamber opposite the glass capillary tubes with the use of constant suction. Changes in Ca^{2+} current amplitude in response to rapidly acting drugs or ionic changes are typically complete in 2–4 min. Switching between separate perfusion syringes, each containing control saline, resulted in no changes in Ca^{2+} current.

Results

Different kinetic properties of low-voltage-activated Ca^{2+} currents of nRT neurones in whole-cell and nucleated patch recordings from soma

To isolate T-type from HVA Ca^{2+} currents, we used an internal solution containing ~ 80 mM F^- , which blocks majority of HVA current in rat sensory neurones (Todorovic & Lingle, 1998; Todorovic *et al.* 2000, 2001). When cells are held (V_h) at -100 mV and depolarized to test potential (V_t) -50 mV, we observed in most of the cells a slowly inactivating T current only in whole-cell configuration (Fig. 1B and C). The difference in size and shape of the T current in nucleated patches *versus* whole-cell recordings from the same cell is shown in Fig. 1B, suggesting that most of the slowly inactivating current originates from dendrites. Immediately after establishing the nucleated patch, currents became smaller and mostly fast-inactivating T current was observed ($n = 17$ cells). Fifteen cells (41%) contained no inactivating inward Ca^{2+} currents in nucleated patch recordings. Figure 1C summarizes experiments from six cells where average traces of T current in whole-cell and nucleated patch are compared. The inactivation time constant (τ) obtained from fitting a single exponential was 54 ± 8 ms in whole-cell and 18 ± 2 ms in nucleated patch recordings ($P < 0.001$). These data strongly suggest that the T currents in dendrites and soma of nRT neurones are distinct and may underlie

different functional properties of somatic and dendritic membranes.

Kinetic properties of T currents in whole-cell and nucleated patch recordings from the soma of nRT neurones in slices

To investigate basic kinetic features of distinct T currents of nRT neurones in brain slices, we performed the experiments summarized in Fig. 2. Figure 2A shows a family of inward currents evoked from $V_h = -100$ mV, to test potential (V_t) from -80 to -40 mV, using whole-cell recordings. Peak inward currents at negative potentials show slow inactivation during a 175 ms long depolarizing pulse.

Figure 2B depicts the typical family of inward T currents in nucleated patches. Current–voltage (I – V) relationships from these experiments indicate that, as in whole-cell recordings from cell soma, the threshold for activation of T current in nucleated patches is around -70 mV and peak current is about -40 mV (Fig. 1C). We noticed only a slight shift to the right of the I – V curve, toward more depolarized potentials in the nucleated patch mode compared with whole-cell mode. Figure 1D represents normalized conductance plotted against voltage curves in whole-cell experiments yielding a V_{50} of -67 ± 1 mV, and a k of 6.6 ± 1.0 mV, and in nucleated patch $V_{50} = -61 \pm 1$ mV and $k = 6.2 \pm 0.8$ mV. Figure 1E compares inactivation τ (obtained by single exponential fits) in five nucleated patches and seven cells from whole-cell recordings. It is evident that inactivation τ (at -70 mV: 147 ± 69 ms for whole-cell and 48 ± 9 ms in nucleated patches, $P < 0.001$) was significantly faster in nucleated patches. Overall, inactivation in nucleated patches became nearly voltage independent at about 20 ms at -50 mV, while in whole-cell recordings this was 57 ms ($P < 0.001$). We observed in only a smaller number of cells (12%) faster inactivating T currents with inactivation τ between 20 and 30 ms in whole-cell recordings, and similarly in only 8% of nucleated patches that had measurable T currents did we notice that inactivation $\tau > 40$ ms (data not shown). Overall, these experiments indicate that dendritic T currents in nRT neurones activate over the similar range of membrane potentials like somatic T currents, but exhibit more than 2.5-fold slower inactivation kinetics than somatic T currents.

Cell-attached recordings from proximal dendrites and somas of nRT neurones

Comparison of our data from whole-cell and nucleated patch recordings suggests that slowly inactivating T current is present predominantly on dendrites of nRT neurones, and that this contributes to observed slow inactivation kinetics in whole-cell recordings. This

conclusion is based on assumption that whole-cell recordings reflect primarily dendritic currents, and that nucleated patches are representative of somatic currents. However, it is possible that observed differences in inactivation kinetics of T current could be the result of an inadequate space-clamp in whole-cell recordings. This led us to examine dendritic and somatic T currents in nRT neurones under identical conditions, using the cell-attached mode of recording, since this method avoids space-clamp problems. Cell-attached recordings, made in the presence of TTX and with a TEA-based barium-rich pipette solution, were used to record ensemble channel activity in soma and proximal dendrites of intact nRT neurones in slices. These experiments demonstrated that an isolated transient inward current was evoked in dendrites in response to voltage steps from $V_h = V_{rest} - 20$ mV to $V_t = V_{rest} + 40$ mV. This inward current resembling slowly inactivating T current seen in whole-cell recordings was clearly discernable in single trials, but is shown even more clearly in an average trace from 20 single trials (Fig. 3B, left panel). The peak of the current was reached at about 60–70 mV positive to holding potential ($V_h = V_{rest} - 20$ mV). Current inactivation kinetics were well described with a single-exponential fit, with inactivation τ measured at about 60 mV positive to V_h of 53 ± 8 ms and the average amplitude of 19.6 ± 2.5 pA ($n = 10$). In contrast, Fig. 3B (middle panel) shows that cell-attached recordings from soma under identical conditions yielded only faster inactivating T current resembling currents obtained in nucleated patch recordings. The average amplitude of T currents in cell-attached recordings from soma was 29 ± 4 pA, and the average inactivation τ only 28 ± 4 ms ($n = 14$, $P < 0.01$). Similarly, Fig. 3B (right panel) shows that inactivation of somatic T currents in nucleated patches recorded in external solution containing 10 mM Ba^{2+} was only slightly different from results obtained in somatic cell-attached recordings (inactivation τ at V_t of -40 mV was 24 ± 2 ms, $n = 6$, $P > 0.05$). Therefore, dendritic T currents had about 2- to 2.5-fold slower inactivation times than currents from soma obtained in cell-attached recordings and nucleated patches (Fig. 3C). Slightly larger depolarizations to $V_t = V_{rest} + 50$ mV did not cause significant changes in inactivation of T currents in either dendritic patches ($\tau 55 \pm 6$ ms) or somatic patches ($\tau 30 \pm 4$ ms) (data not shown). However, in most of the cell-attached patches, even stronger depolarizations evoked a more sustained component of inward current resembling HVA Ca^{2+} currents, and inactivation τ became more complex and better described with multiple components (data not shown). We did not include in our analysis 4 out of 14 dendritic patches (29%) and 20 out of 32 somatic patches (62%) that did not contain measurable ensemble channel currents. In separate set of experiments, we determined that the resting membrane potential (RMP) of soma

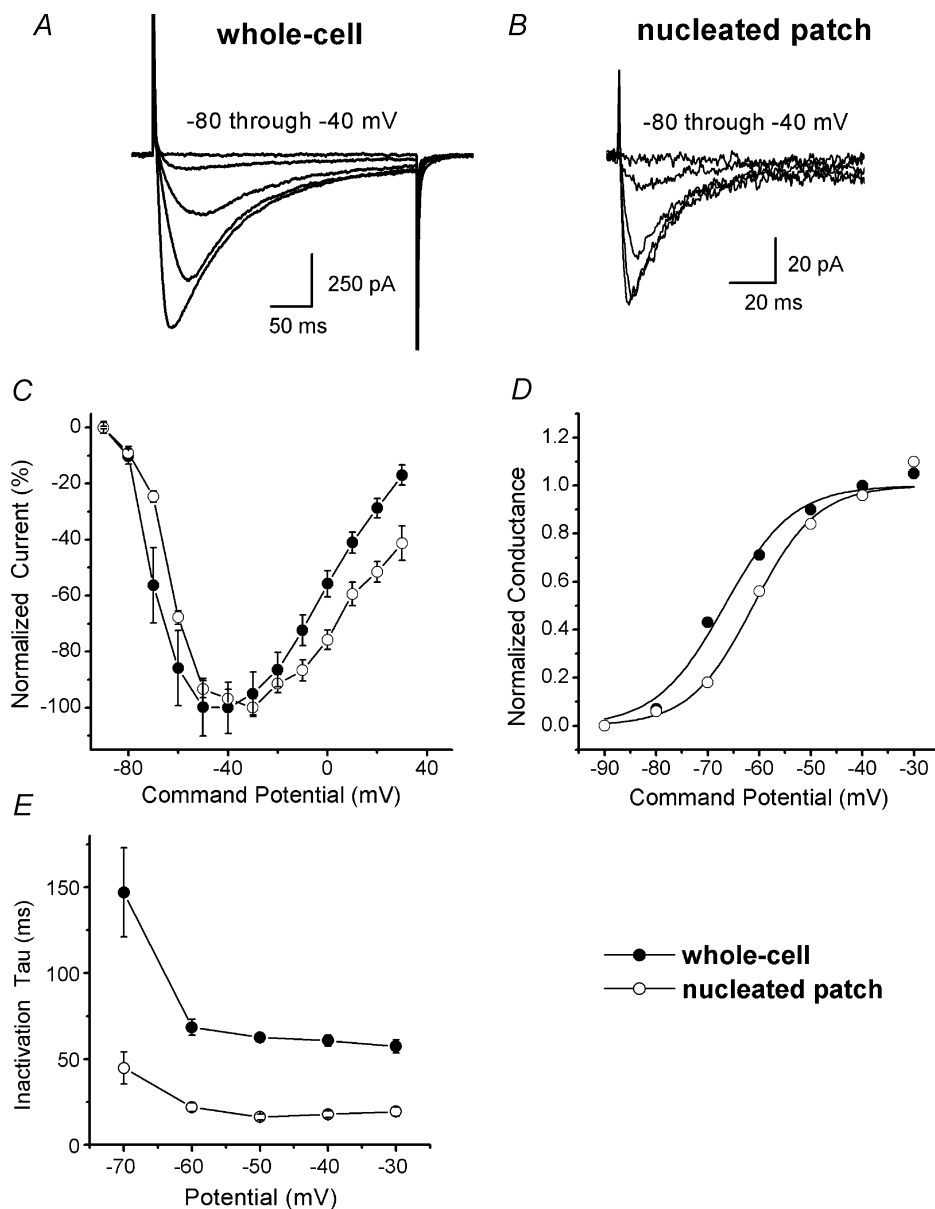


Figure 2. Kinetically distinct subtypes of T-type Ca^{2+} currents are expressed in nRT slices of young rats

A, raw current traces recorded in a whole-cell experiment in response to command steps from a V_h of -100 mV to V_t from -80 to -40 mV. Note that currents start to activate at -70 mV, reaching peak at about -40 mV. The bars indicate calibrations. Note the slow tail currents at the end of depolarizing pulses. **B**, family of inward currents recorded in nucleated patch mode in response to command steps from a V_h of -100 mV to V_t from -80 to -40 mV are averaged from the five nRT cells. Note faster inactivation of T currents in nucleated patch experiments. **C**, normalized peak currents activated at the different command step potentials for whole-cell (●, $n = 7$) and nucleated patch (○, $n = 5$ cells). There is a slight shift of the current–voltage (I – V) curve in nucleated patch mode towards less negative potentials. **D**, the apparent peak conductance values defined as $I_{\text{peak}}/(V - E_r)$ plotted against command potentials in whole-cell ($V_{50} = -67 \pm 1$ mV, $k = 6.6 \pm 0.8$ mV) and in nucleated patch ($V_{50} = -61 \pm 1$ mV, $k = 6.2 \pm 0.8$ mV) from the same cells depicted in Fig. 2C; the extrapolated reversal potential (E_r) was taken to be $+55$ mV. Estimates of V_{50} (half-maximal voltage) and k (the voltage dependence of the distribution) show only small shifts, with up to 20 mV differences in assumed reversal potential values. **E**, inactivation time constants (τ) are plotted against test potentials showing differences in inactivation kinetics between whole-cell and nucleated patch mode: 147 ± 46 ms at -70 mV and 57 ± 4 ms at -30 mV for whole-cell, and 44 ± 9 ms at -70 mV and 19 ± 3 ms at -30 mV for nucleated patch. Note the minimal changes in voltage dependence of inactivation from -60 mV. All points are from the same experiments depicted in Fig. 1C, and vertical bars indicate S.E.M.

(-65 ± 2 mV, $n = 12$) was not statistically different from RMP of dendrites (-67 ± 3 mV, $n = 6$). This suggests that measurements of inactivation τ in our recordings from somatic and dendritic patches were done at corresponding membrane potentials.

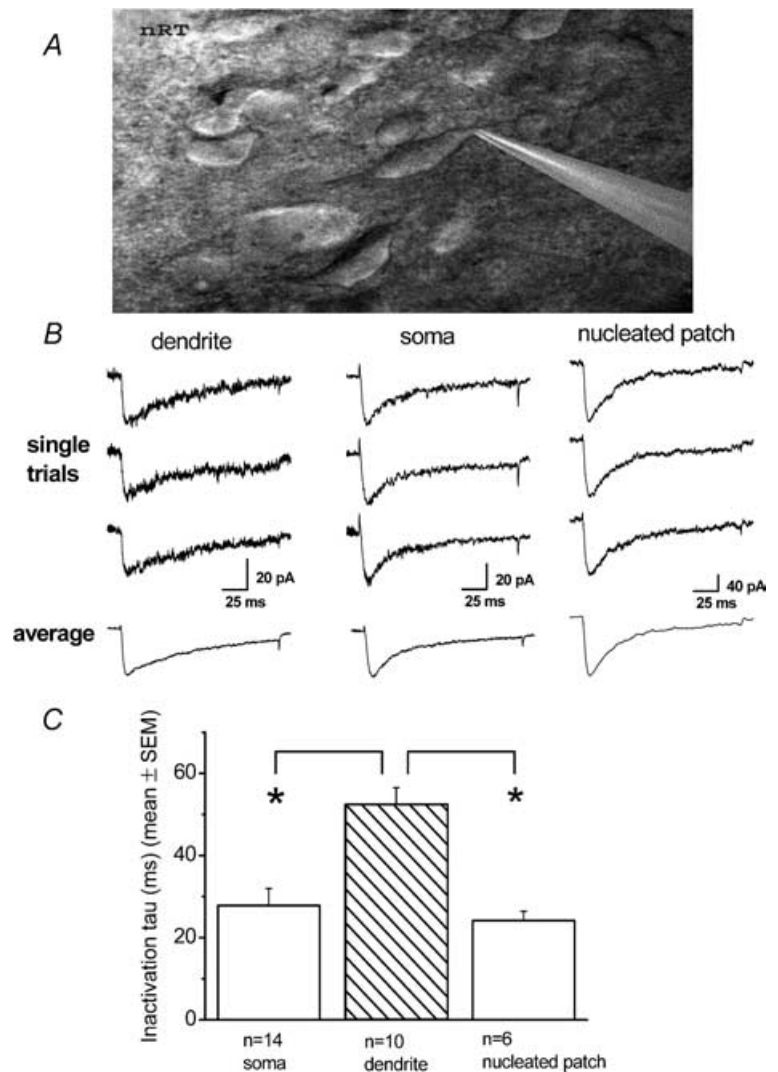
Pharmacological properties of slow T current in nRT neurones

At low concentrations, Ni^{2+} selectively blocks T-type but not HVA Ca^{2+} currents in many native cells. This led us to test sensitivity of slow and fast thalamic T currents in nRT neurones to a range of different concentrations of Ni^{2+} , using whole-cell and nucleated patch recordings. Example currents in whole-cell recordings in control saline and after blockade by $30 \mu\text{M}$ Ni^{2+} and 1 mM Ni^{2+} are shown in Fig. 4A (left panel), and Ni^{2+} inhibits 31 and 87% of peak current, respectively. The time course of blockade and recovery of T-current amplitude during the action of Ni^{2+}

is illustrated in the right panel of Fig. 4A. These plots also illustrate the stability of slow nRT T-type currents under the conditions of these experiments. Figure 4B depicts representative traces (left panel) and time course (right panel) in recordings from nucleated patches showing that $100 \mu\text{M}$ Ni^{2+} blocked about 60% of fast current. Figure 4C summarizes the effects of Ni^{2+} on kinetically different T currents in nRT neurones. In the whole-cell recordings which involve both somatic and dendritic currents, the half-maximal blocking concentration (IC_{50}) was $107 \pm 14 \mu\text{M}$ with a shallow slope indicated by a Hill coefficient of 0.8 ± 0.1 . In the nucleated patch recordings, which include presumably only somatic T currents, the IC_{50} was $64 \pm 4 \mu\text{M}$, with a steep slope indicated by a Hill coefficient of 1.4 ± 0.1 . The twofold shift in IC_{50} in these experiments, combined with the different slopes of concentration–response curves, produced different degrees of slow and fast current inhibition at intermediate Ni^{2+} concentrations (e.g. $300 \mu\text{M}$ Ni^{2+} inhibited somatic

Figure 3. Fast and slowly inactivating T-type Ca^{2+} current in cell-attached and nucleated patch recordings from the soma and proximal dendrites of nRT

A, video image of the neurone shows the position of an electrode recording from the proximal dendrite (magnification $\times 400$). B, left, slowly inactivating T current recorded from the proximal dendrite in cell-attached mode. The top three traces are three consecutive sweeps from an experiment, and the bottom trace is an average from 20 consecutive sweeps in the same cell. To elicit currents, the patch was held at $V_h = V_{\text{rest}} - 20$ mV, and then stepped to $V_t = V_{\text{rest}} + 40$ mV. Single exponential fit of the average trace depicted in this figure gave an inactivation time constant (τ) of 69 ms. B, middle, fast inactivating T current recorded from cell soma in cell-attached mode using the same protocol as outlined above for recordings from dendrites. The top three traces are three consecutive sweeps from an experiment, and the bottom trace is an average from 10 consecutive sweeps in the same cell. Single exponential fit of the average trace depicted in this figure gave an inactivation τ of 32 ms. B, right, fast inactivating T current (V_h of -100 mV and V_t of -40 mV) recorded from cell soma in nucleated patch mode using 10 mM Ba^{2+} in the external solution, as in cell-attached recordings. The top three traces are three consecutive sweeps from an experiment, and the bottom trace is an average from 10 consecutive sweeps in the same cell. Single exponential fit of the average trace depicted in this figure gave an inactivation τ of 26 ms. C, histogram comparing inactivation τ obtained from single exponential fit in experiments in cell-attached recordings from proximal dendrites and somas, as well as nucleated patches. The average inactivation τ in proximal dendrites was 53 ± 8 ms, but only 28 ± 4 ms in cell-attached recordings from soma ($*P < 0.01$) and 24 ± 2 ms in nucleated patch recordings ($*P < 0.001$). The inactivation τ was measured in cell-attached recordings at $V_t = V_{\text{rest}} + 40$ mV, and in nucleated patches at $V_t -40$ mV.



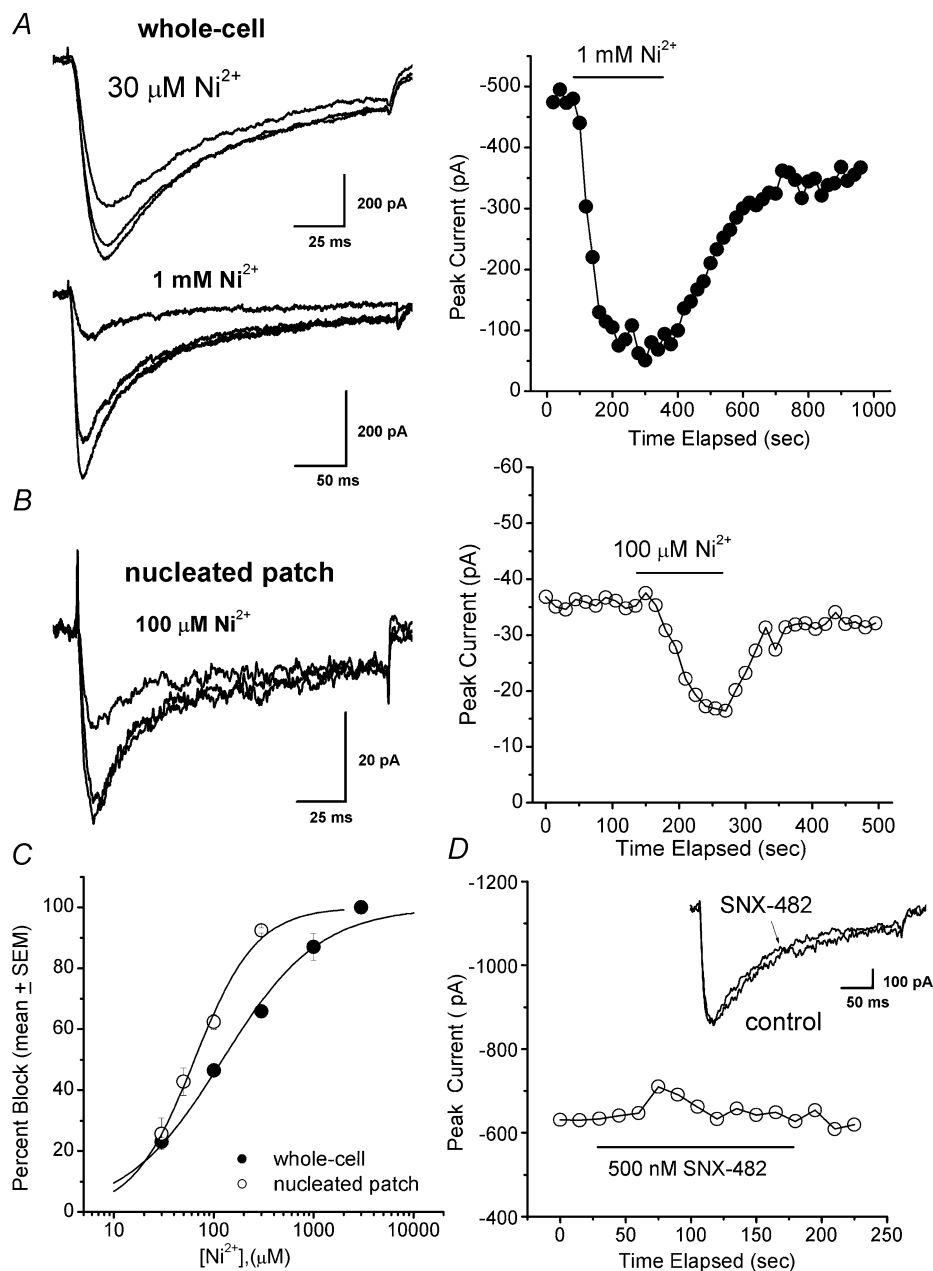


Figure 4. Effects of Ni^{2+} on fast and slowly inactivating T-type Ca^{2+} currents

A, left, whole-cell T current before, during and after application of 30 μM Ni^{2+} (top trace) and 1 mM Ni^{2+} (bottom trace), which inhibit 31 and 87% of peak current, respectively. Bars indicate calibration. **A**, right, time course of onset and recovery of effect of Ni^{2+} is shown for the same cell as in the bottom left panel of **A**. T current was elicited by stepping to -50 mV from a V_h of -100 mV every 15 s. The solid bar denotes the time of application of Ni^{2+} -containing saline. **B**, left, T current before, during and after application of 100 μM Ni^{2+} in a nucleated patch recording, which inhibits about 60% of the peak current. Bars indicate calibration. **B**, right, time course of the onset and recovery of the effect of Ni^{2+} is shown on the same cell as in the left panel of **A**. T current was elicited by stepping to -50 mV from a V_h of -100 mV every 15 s. The solid bar denotes the time of application of Ni^{2+} -containing saline. **C**, concentration–response curves for Ni^{2+} obtained from similar experiments are plotted along with the fitted Hill function (n) for whole-cell experiments (●) and nucleated patch experiments (○). Each point is an average of at least 6 experiments; vertical bars represent s.e.m., and are visible only if they are bigger than the symbols ($n = 21$ cells for whole-cell experiments, and $n = 16$ cells for nucleated patch experiments). Fitted lines correspond to an IC_{50} of 107 ± 14 μM with n of 0.8 ± 0.1 and 100% maximal block for whole cell experiments, and an IC_{50} of 64 ± 4 μM with n of 1.4 ± 0.1 and 100% maximal block for nucleated patch experiments. **D**, time course of application of 500 nM SNX-482 (left), the solid bar indicates the time of application of SNX-482-containing saline in a whole-cell experiment. Insert, traces before and during application of SNX-482 from the same cell showing very little effect on peak and kinetics of slow T current.

T currents more than 90%, but whole-cell current only 60%). Thus, these experiments indicate that fast somatic currents are more sensitive to traditional T-channel blocker Ni^{2+} than slowly inactivating dendritic T currents.

To test the possibility that subtypes of HVA currents might affect measurements of T currents in this study, we applied $5 \mu\text{M}$ ω -MVIIC (a blocker of N-, P-, Q- subtypes of HVA currents, McDonough *et al.* 1996) and found that in five cells this produced an insignificant ($0.8 \pm 1.1\%$, $P > 0.05$) increase in whole-cell T current (data not shown). Similarly, $5 \mu\text{M}$ nifedipine, a representative L-type current blocker, did not significantly affect T current in our whole-cell experiments ($1 \pm 3\%$ block, $n = 3$, $P > 0.05$, data not shown).

In certain instances, R-type HVA currents may resemble T-currents because of somewhat similar kinetic features, such as negative threshold for activation and similar permeation properties, as well as similar pharmacological sensitivities to Ni^{2+} (Randall & Tsien, 1997). SNX-482 is a synthetic peptide that blocks recombinant $\text{Ca}_v2.3$ ($\alpha 1\text{E}$) currents (Newcomb *et al.* 1998), and some native R-type currents (Tottene *et al.* 2000; Breustedt *et al.* 2003). Therefore, we used SNX-482 to elucidate the possible contribution of R-type Ca^{2+} currents in our experiments. Time courses and traces before and after application of 500 nm SNX-482 from the same cell are shown in Fig. 4D, with very little effect on T-type currents in whole-cell recordings. The average effect was only $1 \pm 5\%$ block with 500 nm SNX-482 ($n = 7$ cells, $P > 0.05$). In contrast, in four cells that had only HVA currents ($V_h -60 \text{ mV}$, $V_t -10 \text{ mV}$) that were recorded in the absence of F^- in the recording pipette, this concentration of SNX-482 blocked $16 \pm 2\%$ ($P < 0.01$) of inward current (data not shown). These experiments indicate that known HVA channels do not contribute to slow thalamic T currents in our experimental conditions.

Volatile anaesthetics block slow and fast T currents in nRT neurones in clinically relevant concentrations

It has been shown that general anaesthetics block native and recombinant T channels (Todorovic & Lingle, 1998; Todorovic *et al.* 2000), but the effects of volatile anaesthetics on kinetically distinct T-channel variants within an individual neuronal type have not previously examined. In whole-cell recordings from nRT cells, all fluorinated volatile anaesthetics, such as isoflurane, enflurane, sevoflurane and halothane, reversibly inhibited slow T currents in concentrations ranging from 75 to $1000 \mu\text{M}$ (Fig. 5A). The effects of these volatile agents can be seen in Fig. 5B which represents inward currents evoked from $V_h -100 \text{ mV}$ to V_t of -50 mV every 15 s , before, during and after application of $300 \mu\text{M}$ enflurane (top left), $600 \mu\text{M}$ isoflurane (top right), $600 \mu\text{M}$ halothane (bottom left), and $600 \mu\text{M}$ sevoflurane (bottom right).

We measured effects on inactivation τ for anaesthetic concentrations that block about 50% of T current evoked from $V_h -100 \text{ mV}$ to $V_t -50 \text{ mV}$. Using this protocol, we found that $300 \mu\text{M}$ isoflurane significantly increased the inactivation rate from 49 ± 6 to $27 \pm 2 \text{ ms}$ ($n = 9$ cells, $P < 0.01$), and $150 \mu\text{M}$ enflurane increased inactivation rate from control 63 ± 7 to $42 \pm 5 \text{ ms}$ ($n = 13$ cells, $P < 0.05$). Similarly, $300 \mu\text{M}$ halothane and sevoflurane increased inactivation rate from 70 ± 8 to $40 \pm 2 \text{ ms}$ ($n = 5$ cells, $P < 0.01$) and from 59 ± 5 to $35 \pm 4 \text{ ms}$ ($n = 6$ cells, $P < 0.01$), respectively. This speeding of T-current inactivation induced by volatile anaesthetics may represent features of the channel block, or alternatively may indicate a preferential block of slowly inactivating T-current component by anaesthetics.

In general, anaesthetics were applied and currents recorded until steady-state inhibition was reached before returning to control saline. Aqueous concentrations of four volatile anaesthetics used in this study that correspond to 1 MAC in mammals (minimum alveolar concentration that prevents response to a surgical stimulus in 50% of human subjects) are for room temperature 420 , 720 , 300 and $360 \mu\text{M}$ for isoflurane, enflurane, halothane and sevoflurane, respectively (Franks & Lieb, 1994). Therefore concentrations that block slow thalamic T current are within or, in the case of enflurane, even below those required for surgical anaesthesia.

Next, we wished to examine the hypothesis that volatile anaesthetics might differentially affect kinetically distinct T currents of nRT neurones. To test this possibility, we took advantage of the high lipid solubility and membrane permeability of enflurane, and performed concentration–response experiments in cell-attached recordings from proximal dendrites and somas of nRT neurones. Figure 5C shows that application of $300 \mu\text{M}$ enflurane blocked 85% of dendritic T currents, while Fig. 5D shows that the same concentration of enflurane blocked only 43% of somatic T currents. In a summary of these experiments presented in Fig. 5E, we show that enflurane completely blocked slow dendritic T currents (IC_{50} $135 \mu\text{M}$) with more than twofold higher potency than fast somatic currents (IC_{50} $300 \mu\text{M}$). T currents are evoked in both somatic and dendritic patches at $V_t = V_{\text{rest}} + 40 \text{ mV}$ from $V_h = V_{\text{rest}} - 20 \text{ mV}$. Consistent with this preferential block of slowly inactivating T current, an average concentration–response curve for enflurane in nucleated patch recordings gave an IC_{50} of $290 \pm 16 \mu\text{M}$, and in whole-cell recordings it was about twofold lower, with an IC_{50} of $148 \pm 10 \mu\text{M}$ (Fig. 5F).

It is known that the potency of a certain channel blocker could be influenced by state-dependent features of its effects. Thus, we next investigated whether volatile anaesthetics might alter T-current activation kinetics and availability at different conditioning potentials, effects that could contribute to different potencies in blocking

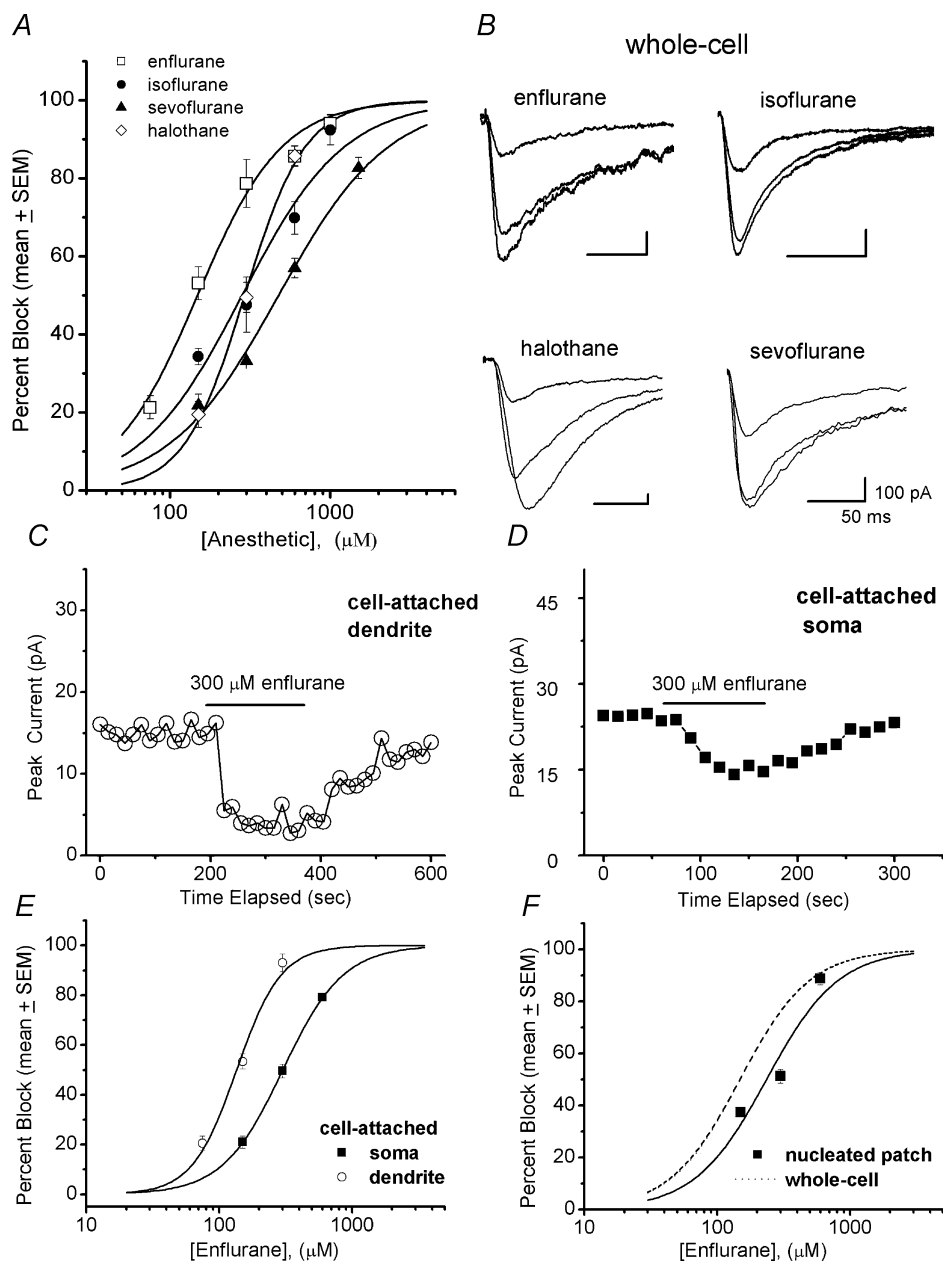


Figure 5. Volatile anaesthetics block slow and fast nRT Ca^{2+} currents in clinically relevant concentrations

A, concentration–response curves showing the different blocking effects of multiple concentrations of enflurane, isoflurane, sevoflurane and halothane in whole-cell recordings. The order of potency was: enflurane ($\text{IC}_{50} = 148 \pm 10 \mu\text{M}$, $n = 1.6$) > isoflurane ($\text{IC}_{50} = 281 \pm 40 \mu\text{M}$, $n = 1.4$) > halothane ($\text{IC}_{50} = 292 \pm 13 \mu\text{M}$, $n = 2.3$) > sevoflurane ($\text{IC}_{50} = 401 \pm 35 \mu\text{M}$, $n = 1.4$). B, representative traces illustrate T-type currents in whole-cell experiments before, during and after application of $300 \mu\text{M}$ enflurane and $600 \mu\text{M}$ of other volatile anaesthetics, as indicated. Bars indicate calibration. Note that all anaesthetics increased the apparent rate of current inactivation. C and D, time courses of onset and recovery of $300 \mu\text{M}$ enflurane in cell-attached recordings from dendrite (C) and soma (D). The horizontal bar indicates the time of application of the anaesthetic. Note that enflurane blocked about 85% of the current in the dendritic recording, while the same concentration of this anaesthetic blocked only about 43% of current in a recording from the soma. E, comparison of concentration–response curves for enflurane in blocking slow dendritic *versus* fast somatic currents in cell-attached recordings. Enflurane induced near complete block of both currents, but dendritic currents were about twofold more sensitive ($\text{IC}_{50} 135 \pm 10 \mu\text{M}$, $n = 2.6 \pm 0.5$) than somatic currents ($\text{IC}_{50} 300 \pm 2 \mu\text{M}$, $n = 1.9 \pm 0.1$). All points are averages from 5 or 6 patches. F, concentration–response curves are plotted for enflurane in whole-cell recordings (dashed line, the same as that depicted in A) and nucleated patch (■), with continuous lines indicating the best fit of Hill plot to each set of points. All points are averages from 4 or 5 cells, and vertical lines indicating s.e.m. are visible only if bigger than the symbols. Enflurane produced near-complete block at maximal concentrations. IC_{50} was $290 \pm 16 \mu\text{M}$ ($n 2.6 \pm 0.4$) in nucleated patch experiments ($n = 13$ cells).

somatic and dendritic T currents in our experiments. Figure 6A depicts average $I-V$ curves in control conditions (●) and during application of $300\ \mu\text{M}$ enflurane (○) in whole-cell recordings ($n = 10$ cells). Figure 6B shows similar experiments with $300\ \mu\text{M}$ enflurane in nucleated patch recordings ($n = 7$ cells). Enflurane in both whole-cell and nucleated patch recordings depressed peak T current at all the potentials tested. However, the inhibitory effect was more pronounced in the whole-cell recordings. The area under the curve was measured using a Gaussian equation (Origin 7.0), which gave an average $61 \pm 2\%$ block in whole-cell experiments, and only $37 \pm 3\%$ in experiments with nucleated patches ($P < 0.001$). However, Fig. 6C and D indicates that the voltage dependence of activation was not significantly changed in these experiments: whole-cell (control average $V_{50} -65 \pm 1$ mV, and enflurane average $V_{50} -63 \pm 1$ mV, $P > 0.05$); nucleated patch (control average $V_{50} -56 \pm 1$ mV, and enflurane average $V_{50} -55 \pm 1$ mV, $P > 0.05$).

Most of the volatile anaesthetics potentiate neuronal GABA_A-mediated Cl⁻ currents (Franks & Lieb, 1994). We were therefore concerned that the apparent reduction of inward current observed with volatile anaesthetics might result from a superimposed GABA_A-receptor-mediated outward current. However, in whole-cell recordings ($n = 5$ cells) following complete block of T current with $3\ \text{mM}$ Ni²⁺, $300\ \mu\text{M}$ enflurane gated no additional current at any potential tested (-60 to $+40$ mV, data not shown). These experiments indicate that the effects of enflurane on T current are specific and do not arise from coincidental activation of an outward Cl⁻ current.

Figure 6E shows the effects of isoflurane (■) and enflurane (○) on steady-state inactivation curves in whole-cell experiments. Both isoflurane and enflurane shifted the inactivation curve toward more negative potentials by about 20 mV (from control of -74 ± 1 to -91 ± 1 mV for enflurane and to -95 ± 1 mV for isoflurane, $n = 7$ cells for each experiment, $P < 0.001$ for both anaesthetics). In contrast, Fig. 6F shows that in nucleated patch experiments enflurane shifted the inactivation curve toward more negative potentials by only 2 mV (from -78 ± 4 to -80 ± 5 mV, $n = 6$ cells, $P > 0.05$). These experiments indicate that volatile anaesthetics stabilize inactive states of the channel, and thus exert a stronger blocking effect at more depolarized conditioning potentials. However, note that this voltage-dependent blocking effect was present only in whole-cell recordings, suggesting that anaesthetics have different mechanisms of block of two kinetically different T currents. This could have contributed to more potent block of enflurane in whole-cell experiments (e.g. Fig. 6A and B, Fig. 5F) and in cell-attached recordings from dendrites that are enriched in slow T currents (Fig. 5E). It has been previously reported that blockade of some T channels by volatile anaesthetics may exhibit voltage-dependent features (e.g.

thalamic relay cells, Ries & Puil, 1999), while effects of volatile anaesthetics on T currents in DRG cells were not voltage dependent (Takenoshita & Steinbach, 1991; Todorovic & Lingle, 1998). Thus, volatile anaesthetic may affect different subtypes of T channels by different mechanisms.

Effects of general anaesthetics on low-threshold Ca²⁺ spikes and burst firing in thalamic slices

The ability of some CNS neurones and particularly thalamic neurones to fire low-threshold Ca²⁺ spikes (LTS) suggested the existence of LVA or T-type Ca²⁺ channels as early as 20 years ago (for review see Llinas, 1988). It has been suggested that slowly inactivating T-type Ca²⁺ currents in nRT neurones underlie LTS, which provide a cellular basis for bursts of action potentials (APs) in nRT neurones that last longer than bursts in thalamic relay neurones (Domich *et al.* 1986; Huguenard & Prince, 1992). Our data indicate that slowly inactivating T-type Ca²⁺ currents are localized predominantly on dendrites of nRT neurones and contribute to slow inactivation kinetics of T currents.

To study the effects of anaesthetics on LTS of nRT neurones, we recorded in whole-cell current-clamp mode with physiological internal solution (see Methods), and $1\ \mu\text{M}$ TTX in external solution to block generation of APs. Under these conditions, when cells are depolarized from about -90 mV by a 50-ms-long direct current injection, slowly developing LTS is critically dependent on negative holding potential and extracellular Ca²⁺ ions, since it is not present if cells are injected with the same depolarizing current at holding potential of -60 mV or in Ca²⁺-free external solution (Fig. 7A, left and middle panels). LTS is also abolished in nucleated patch recordings ($n = 9$) indicating that dendritic currents are necessary for generation of LTS (Fig. 7A, right panel).

Figure 7B shows a typical current-clamp experiment where application of $300\ \mu\text{M}$ Ni²⁺ reversibly and completely blocked LTS in nRT neurones. In a similar experiment depicted in Fig. 7C, $300\ \mu\text{M}$ enflurane reversibly blocked most of the LTS. Enflurane ($300\ \mu\text{M}$) blocked $48 \pm 6\%$ ($n = 6$, $P < 0.001$) and $300\ \mu\text{M}$ Ni²⁺ blocked about $45 \pm 4\%$ of the membrane response to depolarizing current injection (Fig. 7F, left panel, $n = 6$, $P < 0.001$).

In the next set of experiments, external solution did not contain TTX in order to investigate whether inhibition of T currents in voltage-clamp experiments and inhibition of LTS in current-clamp experiments resulted in inhibition of AP burst firing. Figure 7D and E depicts the experiments showing that Ni²⁺ ($300\ \mu\text{M}$) and enflurane ($300\ \mu\text{M}$), in concentrations that profoundly block slow T currents, also diminish excitability of nRT neurones by almost

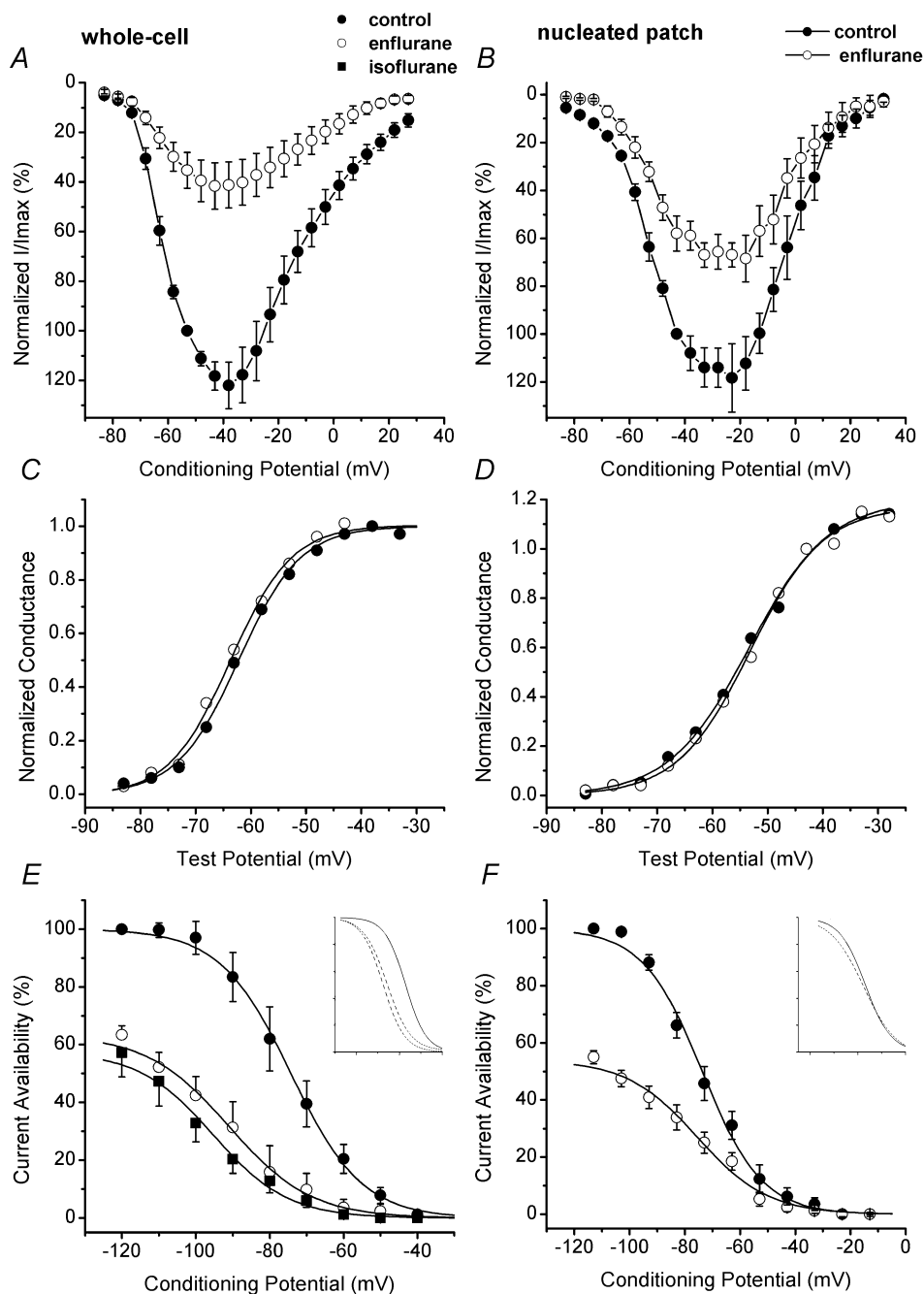


Figure 6. Effects of volatile anaesthetics on steady-state activation and inactivation of T-type currents in nRT neurones in whole-cell and nucleated patch experiments

A and *B*, average *I*-*V* curves in control (●) and in the presence of 300 μM enflurane (○) in whole-cell recordings (*A*, $n = 10$ cells) and nucleated patch recordings (*B*, $n = 7$ cells). Note that enflurane depressed peak current at most potentials, but peak current was more depressed in whole-cell experiments (about 66% block) than in nucleated patch experiments (about 45% block). *C* and *D*, normalized conductance in whole-cell recordings (*C*) and nucleated patch recordings (*D*) calculated from the *I*-*V* experiments depicted above. There is no significant shift of V_{50} in the presence of enflurane (○) from control (●) in either condition. *E* and *F*, the inactivation kinetics of T currents was examined by the steady-state inactivation curves obtained at different conditioning potentials. Conditioning durations of at least 3.5 s are required to achieve apparent steady-state equilibration ($n = 7$, data not shown). Double pulses to -50 mV were used to elicit T currents, separated by 3.5 s prepulses to potentials ranging from -120 to -40 mV before and during application of anaesthetic in whole-cell experiments (*E*) and nucleated patch experiments (*F*). Availability of slow T current for activation is influenced by volatile anaesthetics only in whole-cell experiments. The average fractional availability of T current (conditioning duration of 3.5 s) as a function of voltage is plotted for control (●), 300 μM isoflurane (■) and 150 μM enflurane (○). The best fits of

completely blocking APs generated in a burst. Probability of firing APs was reduced from the average about five to less than one with both enflurane and Ni^{2+} (Fig. 7F, right panel, $n = 6$ for each experiment, $P < 0.001$). In none of these cells did application of Ni^{2+} or enflurane change membrane resting potential or input resistance assessed by injection of a hyperpolarizing pulse. Importantly, the threshold for the first Na^+ spike in the burst measured at the inflection point was not significantly changed by either enflurane (control -54 ± 4 mV, enflurane -56 ± 6 mV, $n = 5$ cells, $P > 0.05$) or Ni^{2+} (control -55 ± 3.0 mV, Ni^{2+} -53 ± 4 mV, $n = 6$ cells, $P > 0.05$).

These data indicate that reduction of slow T current by Ni^{2+} and enflurane may at least contribute to diminished excitability of nRT neurones.

Discussion

Kinetically different subtypes of LVA Ca^{2+} currents are expressed in soma and dendrites of nRT cells in brain slices

Our data directly demonstrate for the first time that kinetically distinct LVA Ca^{2+} channels have differential subcellular distribution in nRT cells. 'Classic' LVA Ca^{2+} currents with fast activation and inactivation kinetics resembling T currents in many other preparations are predominantly expressed in the soma of nRT neurones. However, slowly inactivating T-type Ca^{2+} currents are rare on the soma but are located mostly on the proximal dendrites of nRT neurones. Furthermore, slow inactivation of dendritic T current may allow generation of long-lasting LTS and high-frequency Ca^{2+} -dependent burst firing of nRT neurones.

It was suggested in earlier studies (Destexhe *et al.* 1996) that the properties of dendritic T channels in nRT neurones may differ from those recorded from isolated somas. This was made on the bases of computational modelling and comparison of current properties in isolated soma (dissociated cells) and intact cells in slices. For example, Destexhe *et al.* (1996) reported that inactivation of T currents of neurones in intact slices is slower than in acutely dissociated nRT cells (Huguenard & Prince, 1992). It was suggested that this could be due to the contribution of slower inactivating dendritic T currents in whole-cell recordings in intact slices, or

alternatively due to inadequate space-clamp in whole-cell recordings. Similarly, it was reported that fast and slow inactivating T-current variants exist in slices from the laterodorsal thalamic nucleus (Tarasenko *et al.* 1997). Interestingly, these authors report more cells with a slow current component with maturation of dendritic arbors, which also may suggest that dendritic T currents have slower inactivation than those present on the soma. Our experiments done in cell-attached and nucleated patch recordings are in agreement with previous studies and directly demonstrate that slow T currents are confined to dendrites, while fast T currents are localized in the soma of nRT neurones. Because intact nRT neurones possess long processes, rapid components of current recorded in whole-cell experiments, such as fast-activation kinetics or tail currents (as depicted in Fig. 2A), are not likely to reflect the true amplitude and time course of Ca^{2+} current behaviour. However, all our measurements of amplitudes from holding, peak and steady-state currents are made at time points sufficient to ensure reasonably well-clamped current conditions. Furthermore, it is unlikely that slow inactivation of T currents could be attributed to inadequate space-clamp in whole-cell experiments, since slowly inactivating current was consistently present in our cell-attached recordings from proximal dendrites.

It is interesting that previous studies done with acutely dissociated nRT cells have yielded apparently conflicting results. The study of Tsakiridou *et al.* (1995) reported that nRT neurones have only fast inactivating currents (inactivation τ of 20–30 ms) relatively sensitive to Ni^{2+} ($50 \mu\text{M}$ blocked 38% current). However, the work of Huguenard & Prince (1992) reports that T current in dissociated nRT neurones is somewhat more resistant to Ni^{2+} ($100 \mu\text{M}$ blocked 34% current) and inactivate with a τ of greater than 50 ms as in our whole-cell recordings from soma, as well as our cell-attached recordings from proximal dendrites. In the light of our experiments, it is likely that differences in kinetic and pharmacological properties of T currents in these two studies with acutely dissociated nRT cells are due to different protocols used for cell dissociation, which may have included proximal dendrites in study of Huguenard & Prince (1992).

It is also interesting to speculate on the molecular identity of kinetically distinct T currents in the cell soma

Boltzmann equation in whole-cell experiments (E) yielded a mean V_{50} of -74 ± 1 mV (with slope factor of 9.6 ± 0.4 mV) for control conditions, -95 ± 1 mV (slope factor 10.0 ± 0.8 mV) in the presence of $300 \mu\text{M}$ isoflurane, and -91 ± 1 mV (slope factor 11.1 ± 0.8 mV) in the presence of $150 \mu\text{M}$ enflurane ($n = 7$ cells for each condition, controls are pooled together). In nucleated patch experiments (F), the best fits of Boltzmann equation (continuous line) yielded a mean V_{50} of -74 ± 1 mV (with slope factor of 10.8 ± 0.6 mV) for control conditions, and -76.2 ± 1.3 mV for $300 \mu\text{M}$ enflurane (slope factor 13.1 ± 1.2 mV). Insets represent normalized inactivation curves in control conditions (continuous line) and for enflurane and isoflurane (dashed lines) in whole-cell (E) and enflurane (dashed line) in nucleated patch experiments (F).

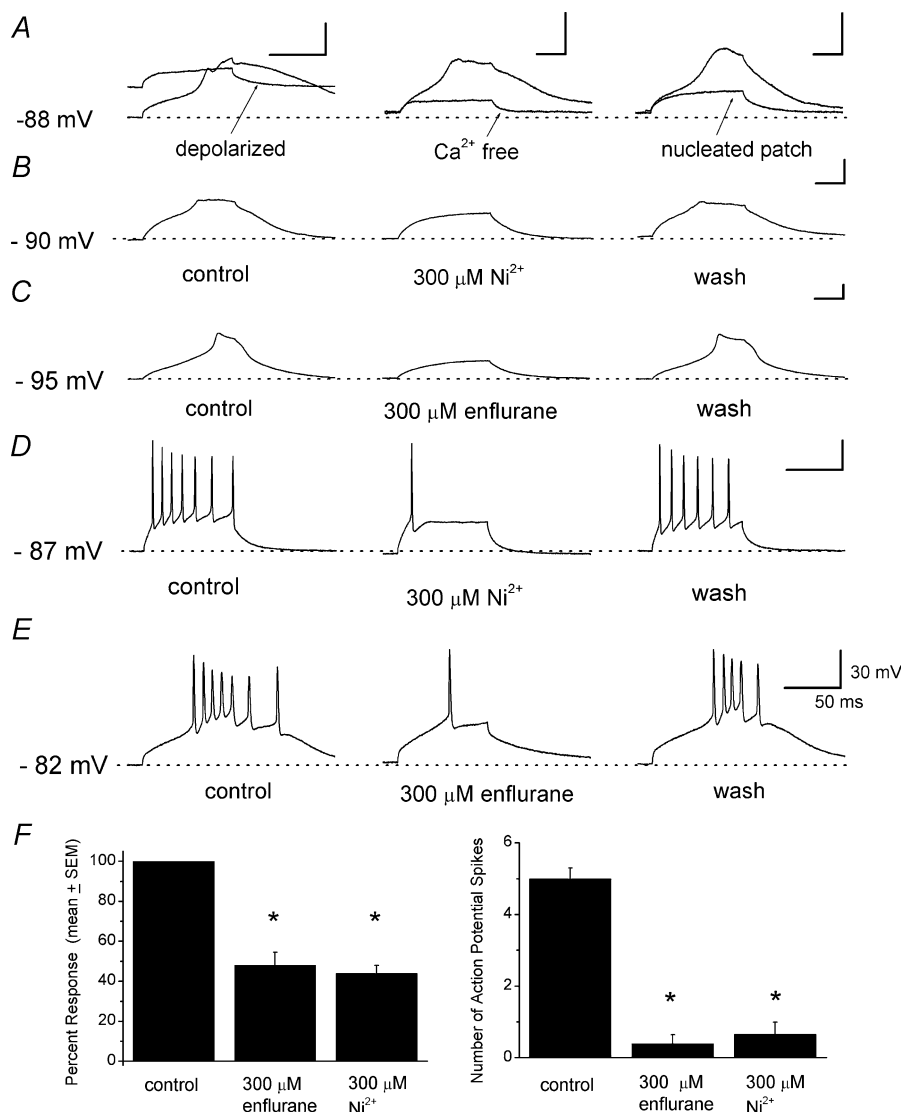


Figure 7. Volatile anaesthetics block LTS and burst firing in whole-cell current-clamp recordings from soma of nRT neurones

A, left, traces indicate prominent low-threshold Ca²⁺ spikes (LTS) evoked with a small membrane depolarization from negative potentials of -86 mV that was not present if the membrane potential of the cell was depolarized to about -60 mV (arrowed trace). Middle, LTS (continuous trace) is absent in the same cells when the extracellular solution did not contain Ca²⁺ ions (arrowed trace). Right, the solid line indicates a robust LTS in a whole-cell recording from an nRT neurone, and the arrowed trace is the trace from the same cell in nucleated patch recording where the identical depolarizing current (60 pA) failed to induce LTS. B, traces from current-clamp experiments show the reversible blocking effect of 300 μ M Ni²⁺ on LTS in a nRT cell in the presence of 1 μ M TTX. C, traces of LTS in another nRT cell in current-clamp mode before (left), during (middle) and after application of 300 μ M enflurane (right), showing a completely reversible blocking effect in the presence of 1 μ M TTX. D, high-frequency burst firing was induced by the injection of a small depolarizing current of 50 ms duration in the absence of 1 μ M TTX in bath solution. The reversible blocking effect of 300 μ M Ni²⁺ on burst of voltage-dependent Na⁺ action potential spikes is indicated by a return of high-frequency firing in the same cell after Ni²⁺ was washed out. E, high-frequency burst firing before (left), during (middle) and after the application of 150 μ M enflurane (right). Enflurane almost completely abolished burst firing. In all cells depicted in A–D, dashed lines indicate stable resting membrane potentials resulting from injected steady hyperpolarizing currents to achieve negative voltages at which LTS is prominent. Values on calibration bars in E apply to all calibration bars presented in this figure. F, histograms showing the average blocking effect of 300 μ M enflurane ($n = 6$ cells) and 300 μ M Ni²⁺ ($n = 6$ cells) on membrane response to small depolarizing current injection. Enflurane blocked $48 \pm 7\%$ and Ni²⁺ blocked $45 \pm 4\%$ of the amplitude of response (left), and comparative blocking effects of 300 μ M enflurane ($n = 6$ cells) and 300 μ M Ni²⁺ ($n = 6$ cells) in relation to number of action potential spikes before and during application of drugs are shown on the right. Vertical bars indicate s.e.m. * $P < 0.001$ in comparison with control conditions.

and dendrites of nRT neurones. Recent cloning of $\alpha 1$ subunits of T channels has revealed the existence of at least three subtypes named G ($\text{Ca}_v3.1$; Perez-Reyes *et al.* 1998), H ($\text{Ca}_v3.2$; Cribbs *et al.* 1998) and I ($\text{Ca}_v3.3$; Lee *et al.* 1999) that are likely to contribute to the heterogeneity of T-type Ca^{2+} currents observed in native cells (Herrington & Lingle, 1992; Todorovic & Lingle, 1998). Among the three subtypes, $\alpha 1\text{I}$ was shown to exhibit slower activation and inactivation kinetics than the $\alpha 1\text{G}$ and $\alpha 1\text{H}$ isoforms, and recent molecular studies suggest that mRNA for both $\alpha 1\text{H}$ and $\alpha 1\text{I}$ isoforms of T channels exist in nRT neurones (Talley *et al.* 1999). Different isoforms of cloned T channels also exhibit different sensitivity to Ni^{2+} , with the $\alpha 1\text{H}$ isoform being about 20-fold more sensitive than $\alpha 1\text{G}$ and $\alpha 1\text{I}$ (Lee *et al.* 1999). We report here that Ni^{2+} exhibited a shallow concentration–response curve ($n=0.8$) and potency in blocking nRT currents in whole-cell recordings (IC_{50} 107 μM), and a somewhat steeper concentration–response curve ($n=1.4$) and higher potency in blocking fast somatic nRT current (IC_{50} 64 μM). Both of these values are in the range between those reported for $\alpha 1\text{H}$ and $\alpha 1\text{I}$ recombinant channels (Lee *et al.* 1999). Given the differences in inactivation kinetics and relative sensitivity to Ni^{2+} , it would be premature to conclude that fast somatic current in nRT neurones may derive from $\alpha 1\text{H}$ channels, and that the slowly inactivating current in proximal dendrites may arise from $\alpha 1\text{I}$ T channel isoforms. Furthermore, it is not clear whether functional expression of channels in native cells correlates well with the presence mRNA of known isoforms, since these channels in native cells may exist in multiple splice variants and can undergo post-translational modifications. Multiple isoforms of T-type $\alpha 1\text{I}$ channels have been described (Murbartian *et al.* 2002), and our recent study indicates that anaesthetic sensitivity of the $\alpha 1\text{Ib}$ splice variant is quite different from native T currents in reticular thalamic neurones (Joksovic *et al.* 2005). Since selective pharmacological and molecular tools for definition of native T-channel isoforms are currently very limited, further molecular and pharmacological studies are needed to better define the kinetically distinct native T-currents in nRT neurones.

Slowly inactivating dendritic T channels in the reticular thalamic nucleus as a possible cellular target for general anaesthetics

It has been generally accepted that anaesthetics depress communication between neurones by either enhancing inhibitory or depressing excitatory drive onto postsynaptic cells. The initial theory proposed that non-specific alteration of the lipid membrane in nerve cells accounts for the anaesthetic state (Meyer, 1899; Overton,

1901). However, research advances in the last two decades suggest that general anaesthetics act through specific sites on the neuronal membrane and that different cellular targets including both ligand- and voltage-gated ion channels appear to be mediating the clinical effects of anaesthetics.

Various components of the anaesthetic state involve a decreased level of arousal (sedation), and loss of consciousness (sleep) and movement (immobilization). In addition, many general anaesthetics induce loss of pain sensation (analgesia), recollection for the event (amnesia), and possess anticonvulsant, muscle-relaxant and anxiolytic properties. It is currently believed that no single end-point of the above-mentioned anaesthetic states is mediated by the effects on a single cellular target (unitary hypothesis). Instead, multi-site hypotheses are proposed, where any particular quality of anaesthetic state is caused by many relevant cellular mechanisms (Urban, 2002; Harrison, 2003; Sonner *et al.* 2003; Rudolph & Antkowiak, 2004). Potentiation of inhibitory GABA_A currents occurs with most halogenated volatile anaesthetics within clinically relevant concentrations (Franks & Lieb, 1994). However, another group of agents called dissociative anaesthetics, such as ketamine and nitrous oxide (laughing gas) (Jevtovic-Todorovic *et al.* 1998), as well as xenon (Franks *et al.* 1998), do not affect GABA_A currents but inhibit *N*-methyl-D-aspartate receptors (NMDARs). Increase in K^+ leak conductance and hyperpolarization of motor neurones by volatile anaesthetics (Sirois *et al.* 1998) could contribute to loss of movement during general anaesthesia. Multiple classes of Ca^{2+} channels exist in nerve cells, and our more recent work (Todorovic & Lingle, 1998; Todorovic *et al.* 2000, 2001), and the work of others (Takenoshita & Steinbach, 1991; Study, 1994; Herrington *et al.* 1991; McDowell *et al.* 1996; Ries & Puil, 1999), indicate that T-type Ca^{2+} channels in both central and peripheral neurones are particularly sensitive to volatile anaesthetics. We report here that volatile anaesthetics inhibit somatic and dendritic T currents in nRT neurones in generally the same, or in the case of enflurane even fourfold lower, concentration range (148 μM) reported for the other relevant targets. However, it is unlikely that inhibition of thalamic T currents in nRT neurones (this study) and thalamic relay neurones (Ries & Puil, 1999) alone can account for any particular end-point of anaesthetic states. Consistent with this, clinical use of an anticonvulsant agent ethosuximide, thought to block T channels in the nRT neurones and thalamic relay neurones in clinically relevant concentrations (reviewed in Huguenard, 1996; Perez-Reyes, 2003; but see also Laresche *et al.* 1998), has not been reported to cause decreased level of arousal. Similarly, direct intrathalamic application of another T channel blocker such as mibefradil in rats (Kim *et al.* 2003) does not induce sleep. However, the thalamus

represents a major 'gateway' of corticothalamocortical functional connections that are essential for cognitive functions, such as learning and memory, as well as vigilance and epileptogenesis (Kinney *et al.* 1994; Llinas *et al.* 1999; McAlonan & Brown, 2002), and it has been shown that most clinically used anaesthetics strongly depress neuronal activity in the thalamocortical system (Rudolph & Antkowiak, 2004). Since dendritic arbors are critical for information processing and integration of synaptic input in the thalamus, preferential blockade of dendritic T currents by anaesthetics may disrupt bidirectional information transfer between the thalamus and cortex, and work in concert with the effects on other ion channels to contribute to anaesthesia-induced loss of sensory perception, amnesia and anticonvulsant properties of anaesthetics.

In conclusion, we show that the two kinetically distinct T-type Ca^{2+} channels exist in nRT neurones, with slowly inactivating current predominantly expressed in proximal dendrites and fast inactivating T current expressed in cell soma. Volatile anaesthetics blocked both fast somatic and slow dendritic T current, and diminished excitability mediated by LTS and burst firing. Thus, given the known role of T-type Ca^{2+} channels in control of neuronal excitability of thalamic cells, the effects of volatile anaesthetics on thalamic T currents may contribute to some important clinical effects of general anaesthetics.

References

- Angel A (1991). Adventures in anaesthesia. *Exp Physiol* **76**, 1–38.
- Breustedt J, Vogt KE, Miller RJ, Nicoll RA & Schmitz D (2003). Alpha1E-containing Ca^{2+} channels are involved in synaptic plasticity. *Proc Natl Acad Sci U S A* **100**, 12450–12455.
- Cribbs LL, Lee J, Yang J, Satin J, Zhang Y, Daud A, Barclay J, Williamson MP, Fox M, Rees M & Perez-Reyes E (1998). Cloning and characterization of $\alpha 1\text{H}$ from human heart, a member of the T-type Ca^{2+} channel gene family. *Circ Res* **83**, 103–109.
- Destexhe A, Contreras D, Steriade M, Sejnowski TJ & Huguenard JR (1996). *In vivo*, *in vitro*, and computational analysis of dendritic calcium currents in thalamic reticular neurons. *J Neurosci* **16**, 169–185.
- Domich L, Oakson G & Steriade M (1986). Thalamic burst patterns in the naturally sleeping cat: a comparison between cortically projecting and reticularis neurons. *J Physiol* **379**, 429–449.
- Franks NP, Dickinson R, de Sousa SL, Hall AC & Lieb WR (1998). How does xenon produce anaesthesia? *Nature* **396**, 324.
- Franks NP & Lieb WR (1994). Molecular and cellular mechanisms of general anesthesia. *Nature* **367**, 607–614.
- Hamill OP, Marty E, Neher E, Sakmann B & Sigworth FJ (1981). Improved patch-clamp techniques for high-resolution current recording from cells and cell-free membrane patches. *Pflugers Arch* **381**, 85–100.
- Harrison NL (2003). Knockin' on the door of general anesthetic mechanisms: but will U.S. researchers be shut out? *Anesth Analg* **97**, 616–618.
- Herrington J & Lingle CJ (1992). Kinetic and pharmacological properties of low-voltage-activated Ca^{2+} current in rat clonal (GH_3) pituitary cell. *J Neurophysiol* **68**, 213–232.
- Herrington J, Stern RC, Evers AS & Lingle CJ (1991). Halothane inhibits two components of calcium current in clonal (GH_3) pituitary cells. *J Neurosci* **11**, 2226–2240.
- Huguenard JR (1996). Low-threshold calcium currents in central nervous system neurons. *Annu Rev Physiol* **58**, 329–358.
- Huguenard JR & Prince DA (1992). A novel T-type current underlies prolonged Ca^{2+} -dependent burst firing in GABAergic neurons of rat thalamic reticular nucleus. *J Neurosci* **12**, 3804–3817.
- Jevtovic-Todorovic V, Todorovic SM, Mennerick S, Powell S, Dikranian K, Benschhoff N, Zorumski CF & Olney JW (1998). Nitrous oxide (laughing gas) is an NMDA antagonist, neuroprotectant and neurotoxin. *Nature Med* **4**, 460–463.
- Joksovic PM, Brimelow BC, Murbartian J, Perez-Reyes E & Todorovic SM (2005). Contrasting anesthetic sensitivities of slow T-type calcium channels of reticular thalamic neurons and recombinant $\text{Ca}_v3.3$ channels. *Br J Pharmacol* **144**, 59–70.
- Kim D, Park D, Choi S, Lee S, Sun M, Kim C & Shin HS (2003). Thalamic control of visceral nociception mediated by T-type Ca^{2+} channels. *Science* **302**, 117–119.
- Kinney HC, Korein J, Panigrahy A, Dikkes P & Goode R (1994). Neuropathological findings in the brain of Karen Ann Quinlan: the role of the thalamus in the persistent vegetative state. *N Engl J Med* **330**, 1469–1475.
- Laresche N, Parri HR, Erdemli G, Guyon A, Turner JP, Williams SR, Asproдини E & Crunelli V (1998). On the action of the anti-absence drug ethosuximide in the rat and cat thalamus. *J Neurosci* **18**, 4842–4853.
- Lee JH, Daud AN, Cribbs LL, Lacerda AE, Pereverzev A, Klockner U, Schneider T & Perez-Reyes E (1999). Cloning and expression of a novel member of the low voltage-activated T-type calcium channel family. *J Neurosci* **19**, 1912–1921.
- Lee JH, Gomora JC, Cribbs LL & Perez-Reyes E (1999). Nickel block of three cloned T-type calcium channels: low concentrations selectively block $\alpha 1\text{H}$. *Biophys J* **77**, 3034–3042.
- Llinas R (1988). The intrinsic electrophysiological properties of mammalian neurons: insight into central nervous system function. *Science* **242**, 1654–1664.
- Llinas RR, Ribary U, Jeanmonod D, Kronberg E & Mitra PP (1999). Thalamocortical dysrhythmia: a neurological and neuropsychiatric syndrome characterized by magnetoencephalography. *Proc Natl Acad Sci U S A* **96**, 15222–15227.

- Magee JC, Christofi G, Miyakawa H, Christie B, Lasser-Ross N & Johnston D (1995). Subthreshold synaptic activation of voltage-gated Ca^{2+} channels mediates a localized Ca^{2+} influx into the dendrites of hippocampal pyramidal neurons. *J Neurophysiol* **74**, 1335–1342.
- Magee JC & Johnston D (1995). Synaptic activation of voltage-gated channels in the dendrites of hippocampal pyramidal neurons. *Science* **268**, 301–304.
- Markram H & Sakmann B (1994). Calcium transients in dendrites of neocortical neurons evoked by single subthreshold excitatory postsynaptic potentials via low-voltage-activated calcium channels. *Proc Natl Acad Sci U S A* **94**, 5207–5211.
- McAlonan K & Brown VJ (2002). The thalamic reticular nucleus: more than a sensory nucleus? *Neuroscientist* **8**, 302–305.
- McCormick DA & Bal T (1997). Sleep and arousal: thalamocortical mechanisms. *Annu Rev Neurosci* **20**, 185–215.
- McDonough GL, Swartz KJ, Mintz IM, Boland LM & Bean BP (1996). Inhibition of calcium channels in rat central and peripheral neurons by ω -conotoxin MVIIC. *J Neurosci* **16**, 2612–2623.
- McDowell TS, Pancrazio JJ, Lynch C & 3rd (1996). Volatile anesthetics reduce low-voltage-activated calcium currents in a thyroid C-cell line. *Anesthesiology* **85**, 1167–1175.
- Meyer H (1899). Zur theorie der alkoholnarkose. *Arch Exp Pathol Pharmacol* **42**, 109–118.
- Murbartian J, Arias JM, Lee JH, Gomora JC & Perez-Reyes E (2002). Alternative splicing of the rat $\text{Ca}(\text{v})$ 3.3 T-type calcium channel gene produces variants with distinct functional properties. *FEBS Lett* **528**, 272–278.
- Newcomb R, Szoke B, Palma A, Wang G, Chen X, Hopkins W, Cong R, Miller J, Urge L, Tarczy-Hornoch K, Loo JA, Dooley DJ, Nadasdi L, Tsien RW, Lemos J & Miljanich G (1998). Selective peptide antagonist of the class E calcium channel from the venom of the tarantula *Hysteroocrates gigas*. *Biochemistry* **37**, 15353–15362.
- Overton S (1901). *Studien Uber die Narkose Zugleich Ein Beitrag Zur Allgemeinen Pharmakologie*. Verlag von Gustav Fischer, Jena.
- Paxinos G & Watson C (1944). *The Rat Brain in Stereotaxic Coordinates*. Academic Press, Australia.
- Perez-Reyes E (2003). Molecular physiology of low-voltage-activated T-type calcium channels. *Physiol Rev* **83**, 117–161.
- Perez-Reyes E, Cribbs LL, Daud A, Lacerda AE, Barclay J, Williamson MP, Fox M, Rees M & Lee J (1998). Molecular characterization of a neuronal low-voltage-activated T-type calcium channel. *Nature* **391**, 896–900.
- Ramon y Cajal (1909). *Histologie Dy Systeme Nerveux de L'homme et Des Vertebres*. Pars, Malonie.
- Randall A & Tsien RW (1997). Contrasting biophysical and pharmacological properties of T-type and R-type calcium channels. *Neuropharmacology* **36**, 879–893.
- Ries CR & Puil E (1999). Mechanism of anesthesia revealed by shunting actions of isoflurane on thalamocortical neurons. *J Neurophysiol* **81**, 1795–1801.
- Rudolph U & Antkowiak B (2004). Molecular and neuronal substrates for general anaesthetics. *Nat Rev Neurosci* **5**, 709–720.
- Sather W, Dieudonne S, MacDonald JF & Ascher P (1992). Activation and desensitization of N-methyl-D-aspartate receptors in nucleated outside-out patches from mouse neurons. *J Physiol* **450**, 643–672.
- Sirois JE, Pancrazio JJ, Lynch C III & Bayliss DA (1998). Multiple ionic mechanisms mediate inhibition of rat motoneurons by inhalation anesthetics. *J Physiol* **512**, 851–862.
- Sonner JM, Antognini JF, Dutton RC, Flood P, Gray AT, Harris RA, Homanics GE, Kendig J, Orser B, Raines DE, Rampil IJ, Trudell J, Vissel B & Eger EI (2003). Inhaled anesthetics and immobility: mechanisms, mysteries, and minimum alveolar anesthetic concentration. *Anesth Analg* **97**, 718–740.
- Steriade M, Deschenes M, Domich L & Mulle C (1985). Abolition of spindle oscillations in thalamic neurons disconnected from nucleus reticularis thalami. *J Neurophysiol* **54**, 1473–1497.
- Stevens WC & Kingston HGG (1992). Inhalation anesthesia. In *Clinical Anesthesia*, 2nd edn, ed. Barash PG, pp. 429–465. J.B. Lippincott, Philadelphia.
- Study RE (1994). Isoflurane inhibits multiple voltage-gated calcium current in hippocampal pyramidal neurons. *Anesthesiology* **81**, 104–116.
- Takenoshita M & Steinbach JH (1991). Halothane blocks low-voltage-activated calcium current in rat sensory neurons. *J Neurosci* **11**, 1404–1412.
- Talley EM, Cribbs LL, Lee J, Daud A, Perez-Reyes E & Bayliss DA (1999). Differential distribution of three members of a gene family encoding low-voltage-activated (T-type) calcium channels. *J Neurosci* **19**, 1895–1911.
- Tarasenko AN, Kostyuk PG, Eremin AV & Isaev DS (1997). Two types of low-voltage-activated Ca^{2+} channels in neurons of rat laterodorsal thalamic nucleus. *J Physiol* **499**, 77–86.
- Todorovic SM, Jevtovic-Todorovic V, Mennerick S, Perez-Reyes E & Zorumski CF (2001). $\text{Ca}(\text{v})$, 3.2 channel is a molecular substrate for inhibition of T-type calcium currents in rat sensory neurons by nitrous oxide. *Mol Pharmacol* **60**, 603–610.
- Todorovic SM & Lingle CJ (1998). Pharmacological properties of T-type Ca^{2+} current in adult rat sensory neurons: effects of anticonvulsant and anesthetic agents. *J Neurophysiol* **79**, 240–252.
- Todorovic SM, Perez-Reyes E & Lingle CJ (2000). Anticonvulsants but not general anesthetics have differential blocking effects on different T-type current variants. *Mol Pharmacol* **58**, 98–108.
- Tottene A, Volsen S & Pietrobon D (2000). Alpha (1E) subunits form the pore of three cerebellar R-type calcium channels with different pharmacological and permeation properties. *J Neurosci* **20**, 171–178.
- Tsakiridou E, Bertollini L, De Curtis M, Avanzini G & Pape H (1995). Selective increase in T-type calcium conductance in reticular thalamic neurons in a rat model of absence epilepsy. *J Neurosci* **15**, 3110–3117.

- Urban BW (2002). Current assessment of targets and theories of anaesthesia. *Br J Anaesth* **89**, 167–183.
- Williams SR & Stuart GJ (2000). Action potential backpropagation and somato-dendritic distribution of ion channels in thalamocortical neurons. *J Neurosci* **20**, 1307–1317.

Acknowledgements

This study was supported by National Institute for Drug Abuse (NIDA) Career Development Awards no. K08-DA00428, and National Institute for General Medical Sciences (NIGMS) grant R01GM070726 to S.T. We thank Dr Steven Mennerick, Dr Charles F. Zorumski, Dr Vesna Jevtovic-Todorovic and Barbara Brimelow for helpful comments on this manuscript.

Different kinetic properties of two T-type Ca²⁺ currents of rat reticular thalamic neurones and their modulation by enflurane

Pavle M Joksovic, Douglas A Bayliss and Slobodan M Todorovic

J. Physiol. 2005;566;125-142; originally published online Apr 21, 2005;

DOI: 10.1113/jphysiol.2005.086579

This information is current as of September 12, 2008

**Updated Information
& Services**

including high-resolution figures, can be found at:
<http://jp.physoc.org/cgi/content/full/566/1/125>

Permissions & Licensing

Information about reproducing this article in parts (figures, tables)
or in its entirety can be found online at:
<http://jp.physoc.org/misc/Permissions.shtml>

Reprints

Information about ordering reprints can be found online:
<http://jp.physoc.org/misc/reprints.shtml>